# Structural, magnetic and electrical properties of the hexagonal ferrites $MFeO_3$ (M = Y, Yb, In)

Lewis J. Downie[1], Richard J. Goff[1], Winfried Kockelmann[2], Sue D. Forder[3], Julia E. Parker[4], Finlay D. Morrison[1] and Philip Lightfoot[1]*

1. EaStCHEM and School of Chemistry, University of St Andrews, St Andrews, Fife, KY16 9ST, UK.
2. STFC ISIS Facility, Rutherford Appleton Laboratory, Chilton, Oxon, OX11 0QX, UK.
3. Materials and Engineering Research Institute, Sheffield Hallam University, City Campus, Sheffield, S1 1WB
4. Diamond Light Source, Ltd., Harwell Science and Innovation Campus, Didcot, Oxfordshire, OX11 ODE, United Kingdom

*Corresponding author, e-mail: pl@st-and.ac.uk

## Abstract

The hexagonal ferrites $MFeO_3$ (M = Y, Yb, In) have been studied using a combination of neutron and X-ray powder diffraction, magnetic susceptibility, dielectric measurements and $^{57}Fe$ Mössbauer spectroscopy. This study confirms the previously reported crystal structure of $InFeO_3$ ($YAlO_3$ structure type, space group $P6_3/mmc$), but $YFeO_3$ and $YbFeO_3$ both show a lowering of symmetry to at most $P6_3cm$ (ferrielectric $YMnO_3$ structure type). However, Mössbauer spectroscopy shows at least two distinct Fe sites for both $YFeO_3$ and $YbFeO_3$ and we suggest that the best model to rationalise this involves phase separation into more than one similar hexagonal $YMnO_3$-like phase. Rietveld analysis of the neutron diffraction data was carried out using two hexagonal phases as a simplest case scenario. In both $YFeO_3$ and $YbFeO_3$, distinct dielectric anomalies are observed near 130 K and 150 K, respectively. These are tentatively correlated with weak anomalies in magnetic susceptibility and lattice parameters, for $YFeO_3$ and $YbFeO_3$, respectively, which may suggest a weak magnetoelectric effect. Comparison of neutron and X-ray powder diffraction shows evidence of long-range magnetic order in both $YFeO_3$ and $YbFeO_3$ at low temperatures. Due to poor sample crystallinity, the compositional and structural effects underlying the phase separation and possible magnetoelectric phenomena cannot be ascertained.

**Keywords:** Hexagonal $YFeO_3$; multiferroic; magnetoelectric; phase separation

## Introduction

The hexagonal polymorph of $YMnO_3$ is one of the most well-studied multiferroic materials, and may be considered the archetypal example of a so-called 'geometric ferroelectric', where the ferroelectricity is a secondary outcome of a purely structural, rather than an electronic instability caused by the coordination requirements at the $Y^{3+}$ site[1-3]. This structure type is relatively rare amongst $ABO_3$ oxides, but is of fundamental interest as it exhibits a B-site having an unusual trigonal bipyramidal coordination (Figure 1). In addition to the magnetic and ferroelectric properties, these compounds have been of recent interest as pigments, due to the chromophoric properties of this unusual coordination[4,5]. It is of interest to compare further examples of this structure type containing transition metals other than $Mn^{3+}$, but there are few options. The hexagonal structure type is stabilised in the case of mixed occupancy of the B-

site by $Cu^{2+}$ and $Ti^{4+}$, $V^{5+}$ or $Mo^{6+}$ (refs. 6-8). The only examples of a full transition metal occupancy other than $Mn^{3+}$ are in the compounds $MFeO_3$ (M = In, Y, Eu – Lu). In the case of Y and Eu – Lu, the thermodynamically-stable phase is the orthorhombic perovskite. The hexagonal polymorph can only be prepared in nanocrystalline form, using methods other than conventional high-temperature solid state routes, for example solution-based precursor methods[9-11], spray-ICP[12] or as an epitaxially-grown thin film[13]. The structural and physical (magnetic and electrical) properties of these ferrites have not been well-studied. The aim of the present work was to shed further light on the behaviour of some of these phases, by probing both their magnetic and electrical behaviour, and attempting to correlate this with crystallographic changes versus temperature.

## Experimental

*Synthesis*

$YbFeO_3$ and $YFeO_3$ were synthesised by a previously reported citrate based method[10]. $Y(NO_3)_3{\cdot}6H_2O$ (99.9%, Sigma Aldrich) (or $Yb(NO_3)_3{\cdot}5H_2O$ (99.999%, Sigma Aldrich)) are dissolved along with a stoichiometric amount of $Fe(NO_3)_3{\cdot}9H_2O$ (99.99%, Sigma Aldrich) in deionised water at ~ 60°C with stirring. Citric acid (99.5%, Sigma Aldrich) is then added in a ratio of 2 moles citric acid to 1 mole metal nitrates. Aqueous ammonia is then added to neutralise the pH. The solution is then allowed to evaporate with stirring at 60 - 80°C until a gel is formed at which point the temperature is increased to ~ 350°C in order to decompose the organic content. After the sample has decomposed to a black/dark brown powder it is calcined in air at 700°C for 10 hours.

$InFeO_3$ was synthesised by a different method involving hydroxide precipitation[14]. Stoichiometric amounts of $InCl_3$ (99.999%, Sigma Aldrich) and $Fe(NO_3)_3{\cdot}9H_2O$ (99.99%, Sigma Aldrich) are dissolved in deionised water. Concentrated ammonia is then added in order to precipitate the metal hydroxides. The mixture is then filtered for the orange suspension, washing with ammonia and deionised water. The filtrate is then allowed to dry in air before calcination at 700°C for 10 hours.

*Powder diffraction*

Preliminary phase purity for each material was confirmed by Rietveld refinement of X-ray powder diffraction data collected on a Stoe STADI/P X-ray diffractometer using Fe-$K_{\alpha 1}$ radiation.

Neutron powder diffraction (NPD) data on $YFeO_3$ and $YbFeO_3$ were collected on the GEM instrument at ISIS. $YbFeO_3$ NPD patterns were collected at 10, 50, 90, 110, 130, 150, 160, 170, 180, 190, 210, 230, 260, 298, 373, 473, 573, 673, 723, 773, 823 and 873 K with each collection time being approximately 40 minutes. Similarly, $YFeO_3$ NPD patterns were collected at 10, 35, 60, 85, 110, 135, 160, 185, 210, 235, 260, 280 and 298 K.

Further X-ray powder diffraction data were collected on beamline I11 at the Diamond Light Source.[15] $InFeO_3$ was studied at 298 K. Low temperature data were collected for $YFeO_3$ at a wavelength of 0.826426(2) Å. Cooling was carried out in a closed cycle helium PheniX cryostat (Oxford Cryosystems) which has been adapted to hold samples in capillary geometry. The powder sample was attached to a 0.5mm diameter copper wire using glycerol and mounted in the cryostat in a specially designed copper block. Data were collected in

constant velocity scanning mode and the cryostat was oscillated about the sample position to give better powder averaging. The sample was scanned for 30 minutes at each temperature after a dwell time of 5 minutes for equilibration and data rebinned after collection to a step size of 5 mdeg.

All quantitative data analysis was carried out by Rietveld refinement using the GSAS program[16] and its EXPGUI user interface.

*Electrical properties*

Dielectric measurements were performed on pressed powder compacts of $YFeO_3$ and $YbFeO_3$. A suitable powder compact of $InFeO_3$ could not be obtained. $YFeO_3$ had platinum electrodes sputtered onto the circular faces of the compacts; $YbFeO_3$ had silver painted electrodes. This allowed for the determination of dielectric constant and dielectric loss between 50 K and 298 K, which was performed between 100 Hz and 10 MHz using an Agilent 4294A AC impedance analyser. Polarisation-field (P-E) measurements were conducted up to ca. 25 kV $cm^{-1}$ and between 1 Hz and 2 kHz using an aixACCT TF2000 analyser.

*Magnetic properties*

Magnetic measurements were conducted on a Quantum Design SQUID MPMS-XL between 4 K and 300 K. Data were recorded in a field of 10,000 Oe while warming the sample from 4 K to 300 K following consecutive zero field cooling (ZFC) and field cooling (FC) cycles. The data were then normalised to the molar quantity of the sample.

*Mössbauer spectroscopy*

$^{57}Fe$ Mössbauer spectroscopy was performed at room temperature using a constant acceleration Wissel spectrometer in transmission mode with a $^{57}Co/Rh$ source and calibrated relative to α-Fe. Lorentzian line fitting was performed using RECOIL software.

**Results**

*Crystallography – neutron powder diffraction*

$YFeO_3$ and $YbFeO_3$ were both studied using NPD at varying temperatures ($YFeO_3$ below ambient and $YbFeO_3$ both above and below ambient). Unfortunately, the data are found to be subject to severe broadening due to the small size of the crystallites under examination. In both cases the structures were modelled at room temperature first (unit cell data available in Supplementary).

$YFeO_3$ was modelled in both the aristotype centrosymmetric $P6_3/mmc$ model and the polar $P6_3cm$ model (with $a \sim \sqrt{3}\ a_p$, $c = c_p$, where $a_p$, $c_p$ represent the aristotype cell parameters), both of which had been proposed in previous studies on $YFeO_3$[5,10]. The $P6_3cm$ model corresponds to the structure adopted by $YMnO_3$ in the ferrielectric phase[3]. In the present case the $P6_3cm$ model unambiguously provides the better fit ($a$ = 6.0728(3) Å and $c$ = 11.7450(14)), specifically fitting additional superlattice peaks at 1.40 and 1.58 Å, as shown in Figure 2(a). Although at first glance the fit looks to be acceptable, closer inspection finds peaks which have not been fitted correctly, especially in the region d = 1.6 – 2.2 Å (Figure

2(b)). Possible reasons for this will be explored further in the Discussion but in order to explore the thermal evolution of the structure, this approximate model in $P6_3cm$ is used. Due to the inherent particle-size broadening and also the approximations in this model, to be clarified later, only lattice parameters were refined as a function of temperature. Between 10 K and ambient it is found that the evolution of the *a* parameter is quite normal, whereas the *c* parameter shows a rather low thermal expansivity (Figure 3). Below 100 K additional peaks appear at high d –spacing (Figure 4) and these are suggested to be magnetic in nature. This postulate is supported by a parallel study by synchrotron X-ray powder diffraction, which is compared further in the Discussion section.

$YbFeO_3$ shows structural behaviour similar to $YFeO_3$ and is also refined in the $P6_3cm$ model at all temperatures (Supplementary). At room temperature, $YbFeO_3$ also shows a fitting anomaly in the range d = 1.6 – 2.2 Å, suggesting again that there is a further subtlety in the phase behaviour. The lattice parameters of $YbFeO_3$ at sub-ambient temperatures (Figure 5) show similar behaviour to $YFeO_3$, but there is a possible anomaly between 100 and 200 K. At high d – spacing, additional peaks are again found to appear below 120 K with a large background also present below 150 K (see Supplementary). High temperature NPD shows that $YbFeO_3$ undergoes a uniform thermal expansion, with no clear anomalies (Supplementary).

Due to problems associated with neutron absorption in In-containing materials, powder X-ray diffraction data only were collected for $InFeO_3$. An adequate Rietveld fit (Figure 6) was obtained in the aristotype $P6_3/mmc$ space group (i.e. $YAlO_3$ or HT-$YMnO_3$ structure type) in agreement with the single crystal structure reported by zur Loye[17]. There were no additional superlattice peaks suggesting any lowering of symmetry, nor any evidence of phase separation. Refined lattice parameters were a = 3.32582(8), c = 12.1912(5) Å; refined atomic parameters are given in the Supplementary.

*Electrical*

Dielectric data show anomalies in both $YFeO_3$ and $YbFeO_3$ at sub-ambient temperatures. Both have the same form of maximum in real part of the permittivity (ε') along with a small maximum in the imaginary part (ε''). The dielectric constant is particularly low for these samples which may be a result of microstructure; due to soft synthesis techniques the resultant crystallite size is very small (~ 10 nm, as measured by TEM).

In the case of $YFeO_3$, a weak maximum in ε' is seen near 130 K (Figure 7(a)). The corresponding dielectric loss peak in this case is not clear due primarily to noise and also because of the approaching lower limit of measurement temperature. The low temperature anomaly is best resolved in $YbFeO_3$ (Figure 7(b)) and is present over the range 18 kHz – 1.8 MHz. The maximum in ε' is broad, but may be indicative of a phase transition centred around 150 K as indicated by the loss peak. It is apparent, however, that there are either magnetic or crystallographic features which are coincident with these low temperature transitions, which will be referred to in the Discussion.

P-E measurements were attempted on both $YFeO_3$ and $YbFeO_3$. In both cases a reliable indication of ferroelectricity was not achieved; behaviour more akin to a linear, slightly lossy dielectric was indicated and cigar-shaped loops were only achieved at high voltage and low frequency. The low frequency loops were found to have a high dielectric loss and are most likely not an indication of ferroelectricity. Such a result does not rule out the possibility of

the sample showing electric ordering, however and we are currently unable to conduct tests to establish the presence of pyroelectricity or piezoelectricity.

*Magnetic*

Magnetic susceptibility versus temperature data were collected for $YFeO_3$, $YbFeO_3$ and $InFeO_3$. $YFeO_3$ and $InFeO_3$ show similar qualitative behaviour and so can be considered together: the $1/\chi$ versus T plot for $YFeO_3$ does not show linearity up to ambient temperature, which would be indicative of Curie – Weiss behaviour (Figure 8(a)). The suggestion that significant antiferromagnetic interactions therefore persist above room temperature is supported by a plot of $\chi T$ against T (Figure 8(b)), which does not reach a paramagnetic plateau. At high temperature the sample should reach magnetic saturation which can be quantified, in the Curie-Weiss regime, by the formula:

$$\chi_m T \approx \frac{\mu^2}{8}$$

For $YFeO_3$ and $InFeO_3$ we would expect a $\chi_m T$ value of 1.879 emu K $mol^{-1}$ for an iron spin of 3/2 and 4.385 emu K $mol^{-1}$ for a spin of 5/2 (the two possible spin states for $Fe^{3+}$ in a trigonal bipyramidal environment). At 300 K we find that $\chi_m T$ is 1.24 emu K $mol^{-1}$ for $YFeO_3$ and 0.925 emu K $mol^{-1}$ for $InFeO_3$ at 300 K. The spin state of the iron cannot be calculated from these data, and higher T data would be required. The magnetic data at low temperature (< 100 K, Figure 8(c)) shows some interesting behaviour and suggests that $YFeO_3$ is not simply antiferromagnetic. A divergence is observed between ZFC and FC data which may be indicative of either weak ferromagnetism or superparamagnetism[18]. Further experiments would be required in order to elaborate on this.

$YbFeO_3$ also does not show Curie-Weiss behaviour nor reach a saturation of $\chi_m T$ up to 300 K (Supplementary). The saturation value at 300 K is 3.35 emu K $mol^{-1}$; in this case the theoretical value (based on non-interacting $Yb^{3+}$ and $Fe^{3+}$ spins; $\mu_{tot}^2 = (\mu_{Fe}^2 + \mu_{Yb}^2)$ and $\mu_{Yb} = 4.54\ \mu_B$) is 4.45 or 6.95 emu K $mol^{-1}$, for $Fe^{3+}$ S = 3/2 or S = 5/2, respectively. Again, it is difficult to draw conclusions about the spin state of the $Fe^{3+}$ from the available data. A divergence in the ZFC versus FC data at low temperature is once again apparent (Supplementary) but not to the same degree as in $YFeO_3$ and not similar to superparamagnetism[18].

*Mössbauer*

The Mössbauer spectra of both $YFeO_3$ and $YbFeO_3$ at room temperature show at least two doublets with isomer shifts indicative of $Fe^{3+}$ (Figure 9, Table 1). The simplest model is to use two doublets although, as discussed later, more complex behaviour cannot be ruled out. The doublets are in an approximate 1:1 ratio, and the derived parameters are in very good agreement with those previously reported by Mizoguchi[12]. In the case of $YFeO_3$ there is a small contribution from a sextet spectrum, which may arise from a corresponding amount of $\alpha$-$Fe_2O_3$ impurity, or perhaps from a superparamagnetic phase of $YFeO_3$: variable temperature Mössbauer studies would be necessary to probe this possibility further. For $InFeO_3$ a single doublet is adequate to fit the observed spectrum, although a marginally better fit could be produced with two doublets; again there is a smaller contribution from an underlying sextet, most likely $\alpha$-$Fe_2O_3$ or from a superparamagnetic phase. Assignment of a single doublet for $InFeO_3$ agrees with the study of Nodari[14]. In the more recent study on

$YFeO_3$ by Subramanian[5] two doublets, with similar derived isomer shifts and quadrupole splittings, are again observed, but in this case the fits suggest two $Fe^{3+}$ sites in the ratio 78/22 %. Interestingly, for a sample of composition $YFe_{0.3}In_{0.7}O_3$ in that study a single doublet site was observed; note that in this case $In^{3+}$ occupies the B-site rather than the A-site.

## Discussion

*A. Two – Phase Model*

There is a clear inconsistency between the structural and Mössbauer results; the $P6_3cm$ model requires only one crystallographically unique Fe site, which appears to contradict the information suggesting at least two sites from the Mössbauer data. We also note that there is no evidence for a significant amount of crystalline $Fe_2O_3$ from the neutron data, which may support the suggestion that the sextet in the Mössbauer spectrum is associated with a superparamagnetic $YFeO_3$ phase.

Two possibilities were therefore explored in order to provide a more satisfactory model: (i) lowering of symmetry to one of the hexagonal/trigonal subgroups of $P6_3cm$, keeping the unit cell metrics the same (ii) a fit using two very similar hexagonal phases ($P6_3cm$) having the same fixed composition and atomic parameters constrained to be equal, but differing lattice parameters. This is, of course, an approximation; the two phases should have at least slightly different local Fe environments, but it is not reasonable to attempt to model these differences given the subtlety of the effects seen in our diffraction data. For option (i) each of the subgroups $P6_3$, P3c1 and P31m were considered, but only P31m allowed two Fe sites in a 1:1 ratio. However, the improvements in fit were not significant (see Supplementary for further details) and, in particular the additional peak near d = 1.98 Å (Figure 2(b)), is not fit satisfactorily. For option (ii) a significant improvement in fit was achieved, with $\chi^2$ and $R_{wp}$ values of 4.90, 0.032 versus 3.65, 0.027 for single phase versus two phase fits, respectively over one histogram (Figures 2(b) and 10).

The lattice parameters of the two phases refined as a = 6.0689(17) c = 11.696(3) Å and a = 6.078(2), c = 11.835(5) Å, respectively. Phase fractions for the two phases could be derived as approximately 60/40 %, which are in good agreement with the present Mössbauer results. Given that our own Mössbauer results and those of Mizoguchi[12] suggest 57/43 (discounting the sextet) and 55/45 % (for $YbFeO_3$), respectively, but those from Subramanian[5] suggest 78/22 %, it therefore seems most likely that the cause of the two sites seen in the Mössbauer studies is a phase separation, the extent of which may be dependent on the details of the synthesis, rather than a lowering of crystallographic symmetry. The phase separation may occur for a variety of reasons. One possibility is a difference in composition, e.g. oxygen content, although this is unlikely as it would be assumed that one would see the presence of $Fe^{2+}$ in the Mössbauer spectra. Another more likely explanation is a size or strain effect either manifesting itself as a critical particle size below which one structure is adopted and above another (as suggested by Subramanian[5]) or a core – shell model in which surface unit cells may be a different size from the bulk. More physically realistic is a model allowing a range of cell sizes to be present in a relaxation type mechanism and we are just seeing/modelling the extremes. These features require further exploration. Further details of the two-phase refinement model are given in the Supplementary information.

*B. Magnetic – Electrical – Structural Link*

Although the exact structural details of $MFeO_3$ have proven difficult to determine it is clear that they show some interesting features magnetically and electrically. The electrical anomaly present in $YFeO_3$ appears to be consistent with a very subtle change in magnetism. This is best shown with a plot of the dielectric data alongside the derivative of $1/\chi$ vs T (Figure 11(a)). This indicates a possible link between magnetic and electrical properties and possibly a magnetoelectric effect. The same effect is not apparent in $YbFeO_3$ however (Figure 11(b)). What is found in $YbFeO_3$ is a possible link between the dielectric anomaly and lattice parameters. The anomalous trend in the a-parameter is discernible in the range $100 < T < 200$ K, which may be associated with the observed electrical feature near 150 K (Figure 12). Two of the most distinctive structural degrees of freedom[3] which differentiate the $P6_3cm$ model from the parent $P6_3/mmc$ model are the relative displacements of the $Y^{3+}$ cations along the z-axis and the tilting of the $FeO_5$ polyhedron. Plots of these two parameters versus temperature (see Supplementary) for $YbFeO_3$, based on a single $P6_3cm$ phase model, show continuous trends, except for a possible feature in the tilt angle below 200 K. Whilst it is possible that this may also correlate with the observed electrical anomaly, the approximations in the structural model must be borne in mind. In $YFeO_3$ this structural response cannot be seen within the resolution of the experiment.

In both cases the dielectric anomaly is found to be coincident with an increase in background in the NPD patterns at high d – spacing (between 3.5 and 5.5 Å). This is possibly related to some short – range magnetic order or a short – range structural effect which is yet to be determined.

*C. Low Temperature Magnetic Structure and Properties*

For $YFeO_3$ an additional low temperature powder X-ray (synchrotron) diffraction experiment was carried out, in order to clarify whether the additional peaks observed below ~100 K in the NPD were of magnetic or structural origin. Comparisons of the key long d-spacing regions of the NPD and X-ray data at 298 K and 30 K are shown in Figure 13. It is clear that the dominant additional peak (100) near d = 5.2 Å observed in the NPD pattern is completely absent in the X-ray pattern. We therefore conclude that this peak is due, predominantly, to magnetic scattering, and necessitates long-range magnetic order, despite the lack of a clear signal in the susceptibility data. A similar observation of magnetic peaks by NPD, in the absence of a clear anomaly in susceptibility, has been reported in the analogue, $YbMnO_3$[19].

Fitting of the peaks appearing at low temperature in the NPD data by various magnetic models was therefore attempted, but with limited success. Using a magnetic unit cell of the same size as the crystallographic one there are six possible Shubnikov groups for $YMnO_3$ which can also be applied to $YFeO_3$; $P6_3cm$, $P6_3'c'm$, $P6_3'cm'$, $P6_3c'm'$, $P6_3$ and $P6_3'$ (Ref. 20). Poor agreement is observed in each case (Supplementary), in particular a very weak peak at d ~ 4.5 Å remains un-indexed without an expansion of the unit cell. Due to the relatively poor data quality and the likelihood of phase separation (discussed above) no convincing magnetic structural model could be derived.

Fitting of trial magnetic structures by Rietveld refinement was also attempted for $YbFeO_3$ with the same models as for $YFeO_3$. In this case there were no clearly un-indexed peaks, and the suggested Shubnikov groups do account for the presence of the observed peaks, but the quality of fit was again poor and indecisive (Supplementary). The $Yb^{3+}$ moments were not taken into account in these fits. As an example, the refined magnetic moment for the Fe site was 1.88 $\mu_B$ in the Shubnikov group $P6_3c'm'$, which allows a ferromagnetic component along

z; the other groups give only marginally poorer fits, however. In previous work on hexagonal $YMnO_3$ it has been shown that it is virtually impossible to distinguish between the various possible magnetic symmetries based purely on powder diffraction data; polarised neutron studies on single crystals are required[20]. Of course, from the present experiment we cannot rule out the possibility that the additional peaks at low temperature are purely structural in origin in the case of $YbFeO_3$, caused by reduction of crystallographic symmetry to e.g. $P6_3$. However, two recent studies[21,22] of $YbFeO_3$ in thin-film form suggest evidence for long-range magnetic order up to at least 50 K. One of these studies[21] also shows evidence for a secondary dielectric transition and corresponding magnetocapacitive effect, near 220 K, which may correspond to our observed lattice parameter anomaly.

Two further features of the additional scattering at lower temperature in both $YFeO_3$ and $YbFeO_3$ are worthy of note; (i) for both materials there appears to be an increase in the background scattering in the vicinity of the additional high-spacing peaks as the temperature is lowered (Figure 4 and Supplementary). This may be due to some short-range ordering, presumably magnetic in origin if the peaks are indeed magnetic Bragg peaks. (ii) Fits to the intensities of single peaks, such as the (100) near d = 4.8 Å in $YbFeO_3$, show a continuously increasing intensity towards low temperature (Figure 14(a)) rather than a saturation, as would be expected for normal magnetic ordering. This contrasts with the corresponding behaviour seen for $YFeO_3$ (Figure 14(b)), which does show a normal tendency towards saturation. The behaviour in $YbFeO_3$ may be due to some 'triggering' of the ordering of the $Yb^{3+}$ sublattice induced by ordering of the $Fe^{3+}$ sublattice. This sort of phenomenon has previously been reported in $HoMn_2O_5$[23].

**Summary and Conclusions**

This multi-technique study of the hexagonal ferrites $MFeO_3$ (M = Yb, Y, In) supports several observations previously made on these systems, and sheds some new light on their phase behaviour and physical properties. We also open up several new lines for further investigation. In line with the previous single crystal study[17], we observe that $InFeO_3$ adopts the aristotype $P6_3/mmc$ structure at ambient temperature. This is in contrast to the analogue $InMnO_3$, where single crystal[24] and bulk polycrystalline[25] studies appear to show the existence of $P6_3/mmc$ and $P6_3cm$ polymorphs, respectively. Both $YFeO_3$ and $YbFeO_3$ are shown to adopt the $P6_3cm$ structure at ambient temperature, however, both show a subtle phase separation which can be modelled simply as two very similar hexagonal phases. Due to problems inherent in the diffraction data, related to the poorly crystalline nature of the materials, it is not possible to make a definitive assessment of the differences between the two phases, or the origins of the phase separation. Nevertheless, the proposed phase separation model is consistent with the previous and present observations of at least two Fe sites from Mössbauer studies, and the fact that the ratios of these differ in different studies (which rules out models based on symmetry lowering within a single phase).

Our dielectric studies reveal anomalies below ambient temperature in both $YFeO_3$ and $YbFeO_3$. In the case of $YFeO_3$, this is tentatively linked to a very subtle anomaly in magnetic susceptibility, and the appearance of additional (apparently magnetic) Bragg peaks in the neutron diffraction data; for $YbFeO_3$ the electrical anomaly corresponds to an anomaly in lattice parameters versus temperature. This may be suggestive of some weak magneto-electric behaviour in each system, although once again these correspondences are not clear-cut, and definitive conclusions cannot be drawn.

Further synthetic work will be required in order ascertain whether it is possible to prepare better crystalline materials in these systems, which may allow a more thorough characterisation of their crystallographic nature, which in turn may allow more precise and detailed correlations of structure/composition and physical properties.

**Acknowledgements**

We thank EPSRC for funding, STFC for providing neutron facilities and Diamond Light Source for provision of synchrotron facilities. We thank Dr Chiu Tang for assistance at Diamond and Dr A. Kusmartseva (University of Edinburgh) for assistance with the SQUID measurements. FDM thanks the Royal Society for a Research Fellowship.

**References**

1. B. B. van Aken, T. T. M. Palstra, A. Filippetti and N. A. Spaldin, Nature Mater., 3 (2004) 164.
2. C. J. Fennie and K. M. Rabe, Phys. Rev. B., 72 (2005) 100103.
3. A. S. Gibbs, K. S. Knight and P. Lightfoot, Phys. Rev. B., 83 (2011) 094111.
4. A. E. Smith, H. Mizoguchi, K. Dlaney, N. A. Spaldin, A. W. Sleight and M. A. Subramanian, J. Amer. Chem. Soc., 131 (2009) 17086.
5. P. Jiang, J. Li, A. W. Sleight and M. A. Subramanian, Inorg. Chem., 50 (2011) 5858.
6. N. Floros, J. T. Rijssenbeek, A. B. Martinson and K. R. Poeppelmeier, Solid State Sciences, 4 (2002) 1495.
7. V. Kataev, A. Möller, U. Löw, W. Jung, N. Schittner, M. Kriener and A. Freimuth, J. Magn. Magn. Mater., 290-291 (2005) 310.
8. S. Malo, A. Maignan, S. Marinel, M. Hervieu, K. R. Poeppelmeier and B. Raveau, Solid State Sciences, 7 (2005) 1492.
9. O. Yamaguchi, H. Takemura, M. Yamashita and A. Hayashida, J. Electrochem. Soc., 138 (1991) 1492.
10. J. Li, U. G. Singh, T. D. Schladt, J. K. Stalick, S. L. Scott and R. Seshadri, Chem. Mater., 20 (2008) 6567.
11. L. Wu, J. C. Yu, L. Zhang, X. Wang and S. Li, J. Solid State Chem., 177 (2004) 3666.
12. Y. Mizoguchi, H. Onodera, H. Yamauchi, M. Kagawa, Y. Syono and T. Hirai, Mater. Sci. Eng., A217-218 (1996) 164.
13. A. A. Bossak, I. E. Graboy, O. Yu. Gorbenko, A. R. Kaul, M. S. Kartavtseva, V. L. Svetchnikov and H. W. Zandbergen, Chem. Mater., 16 (2004) 1751.
14. I. Nodari, A. Alebouyeh, J. F. Brice, R. Gerardin and O. Evrard, Mater. Res. Bull., 23 (1988) 1039.
15. S.P. Thompson, J. E. Parker, J. Potter, T. P. Hill, A. Birt, T. M. Cobb, F. Yuan, C. C. Tang, Rev. Sci. Instr., 80, 075107 (2009)
16. A. C. Larson and R. B. Von Dreele, Los Alamos National Laboratory Report No. LA-UR-86-748, 2000 (unpublished).
17. D. M. Giaquinta, W. M. Davis and H.-C. zur Loye, Acta Crystallogr., C50, (1994) 5.
18. M. Vettraino, X. He, M. Trudeau and D. M. Antonelli, J. Mater. Chem., 11 (2001) 1755.
19. X. Fabrègas, I. Mirebeau, P. Bonville, S. Petit, G. Lebras-Jasmin, A. Forget, G. André and S. Pailhès, Phys. Rev. B, 78 (2008) 214422
20. P. J. Brown and T. Chatterji, J. Phys. Condens. Matter, 18 (2006) 10085.
21. Y. K. Jeong et al., preprint.
22. H. iida, T. Koizumi and Y. Uesu, Phase Transitions, 84 (2011) 747.

23. G. Beutier, A. Bombardi, C. Vecchini, P. G. Radaelli, S. Park, S.-W. Cheong and L. C. Chapon, Phys. Rev. B, 77 (2008) 172408.
24. D. M. Giaquinta and H. C. zur Loye, J. Amer. Chem. Soc., 114 (1992) 10952.
25. J. E. Greedan, M. Bieringer, J. F. Britten, D. M. Giaquinta and H. C. zur Loye, J. Solid State Chem., 116 (1995) 118.

**Table 1** Mössbauer parameters for $InFeO_3$, $YFeO_3$ and $YbFeO_3$determined at ambient temperature (Parameters have an uncertainty of ± 0.02 mm/s.)

| **$YFeO_3$** | | | | | |
|---|---|---|---|---|---|
| | CS (mm/s) | QS (mm/s) | w+ (mm/s) | w-/w+ | Area (%) |
| Doublet 1 | 0.29 | 2.13 | 0.22 | 1 | 52.5 |
| Doublet 2 | 0.30 | 1.18 | 0.37 | 1 | 39.7 |
| | CS (mm/s) | ε (mm/s) | H (T) | w3 (mm/s) | Area (%) |
| Sextet | 0.02 | 0.00 | 32.8 | 0.22 | 7.80 |
| **$YbFeO_3$** | | | | | |
| | CS (mm/s) | QS (mm/s) | w+ (mm/s) | w-/w+ | Area (%) |
| Doublet 1 | 0.29 | 1.82 | 0.23 | 1 | 56.5 |
| Doublet 2 | 0.31 | 1.01 | 0.25 | 1 | 43.5 |
| **$InFeO_3$** | | | | | |
| | CS (mm/s) | QS (mm/s) | w+ (mm/s) | w-/w+ | Area (%) |
| Doublet 1 | 0.31 | 0.75 | 0.32 | 0.92 | 89.3 |
| | CS (mm/s) | ε (mm/s) | H (T) | w3 (mm/s) | Area (%) |
| Sextet 1 | 0.37 | -0.12 | 49.3 | 0.28 | 10.7 |

**Figures**

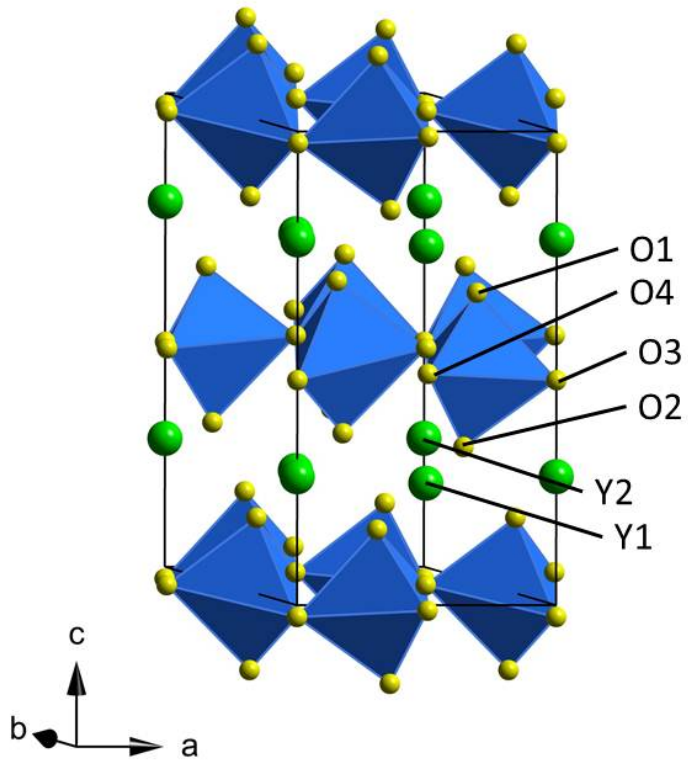


**Figure 1** The ferrielectric $YMnO_3$ structure type, space group $P6_3cm$.

a)

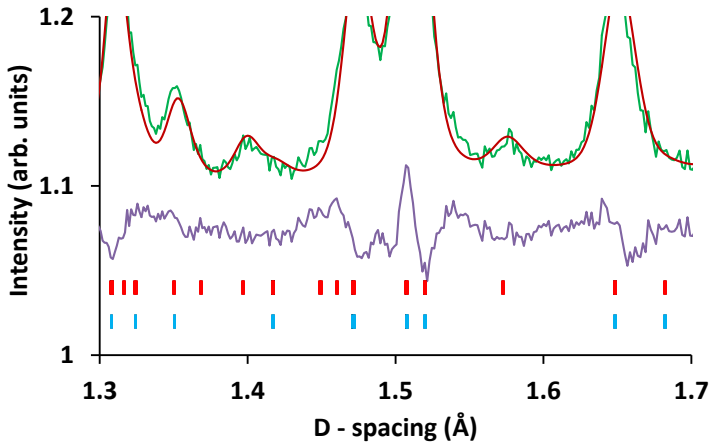


b)

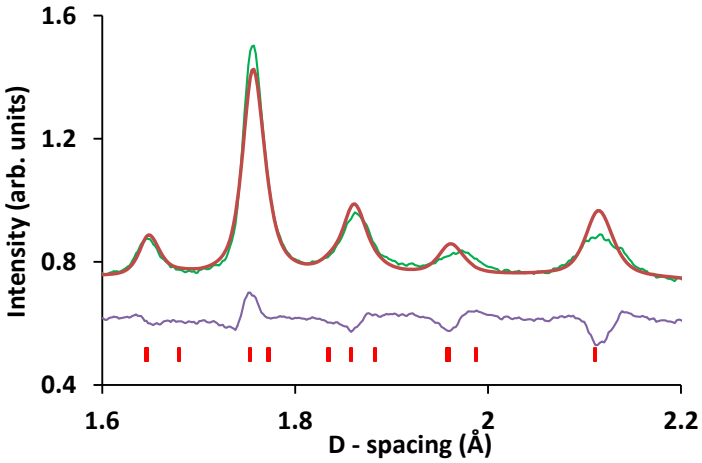


**Figure 2** Portions of the Rietveld fits to the NPD data for $YFeO_3$ at room temperature. (a) Single $P6_3cm$ phase (upper tick marks), showing peaks not fit by the aristotype $P6_3/mmc$ model (lower tick marks) (b) region of poor fit suggesting that the single-phase $P6_3cm$ model is not quite correct.

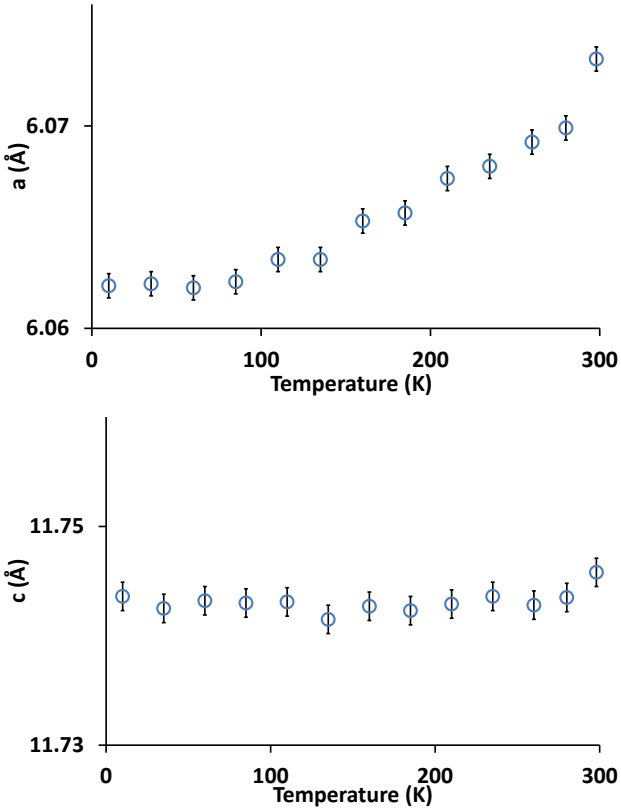


**Figure 3** Lattice parameters a and c versus temperature (sub-ambient) for $YFeO_3$

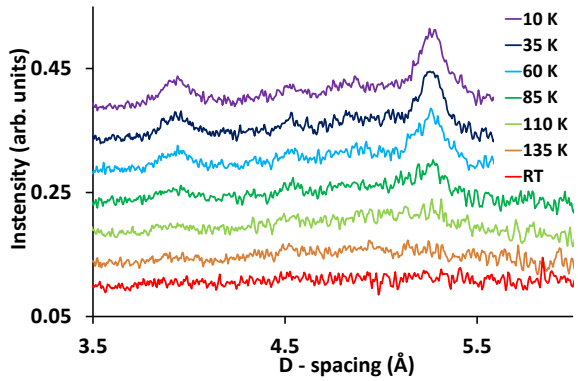


**Figure 4** Expansion of the raw NPD data at long d-spacings for $YFeO_3$, showing the appearance of magnetic Bragg peaks

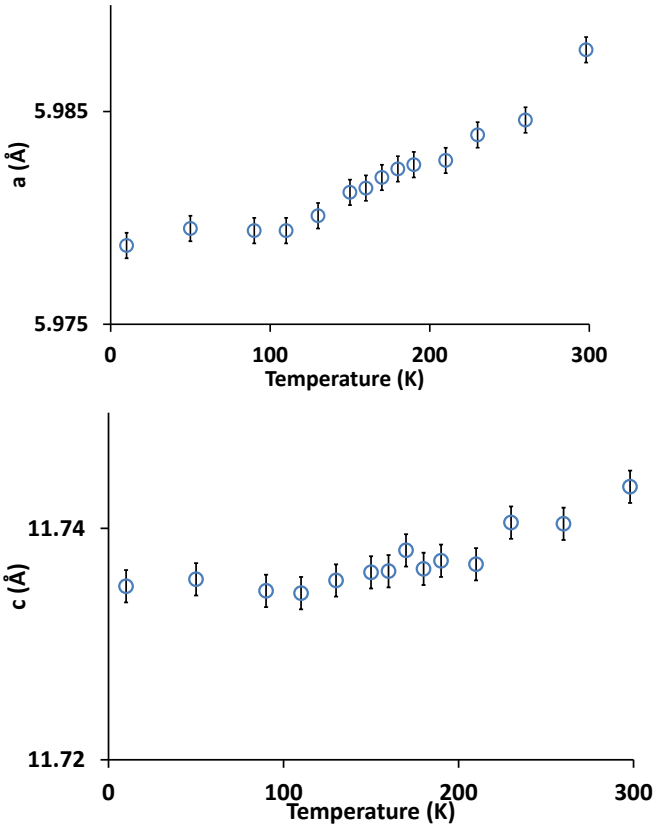


**Figure 5** Lattice parameters a and c versus temperature (sub-ambient) for $YbFeO_3$

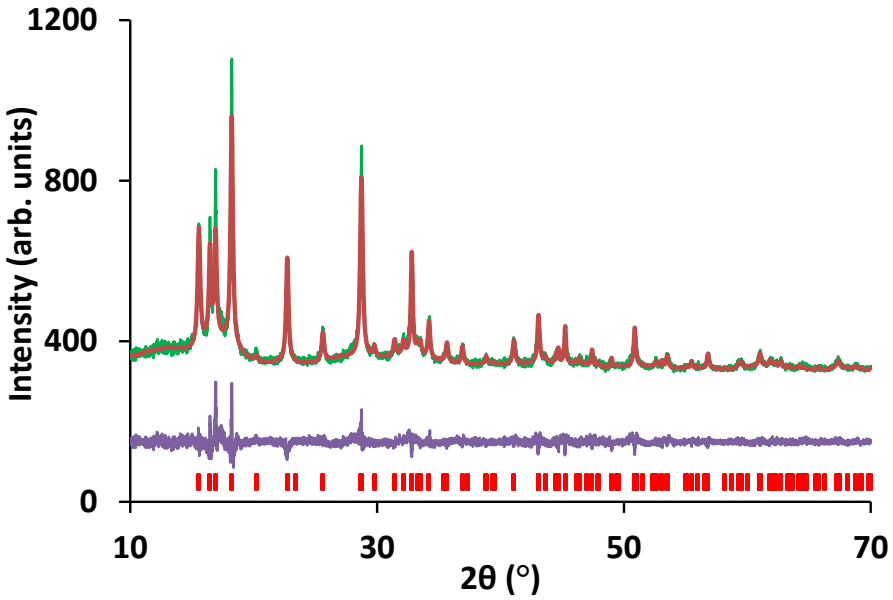


**Figure 6** Rietveld fit for $InFeO_3$, in the aristotype $P6_3/mmc$ model, from synchrotron PXRD at room temperature.

(a)

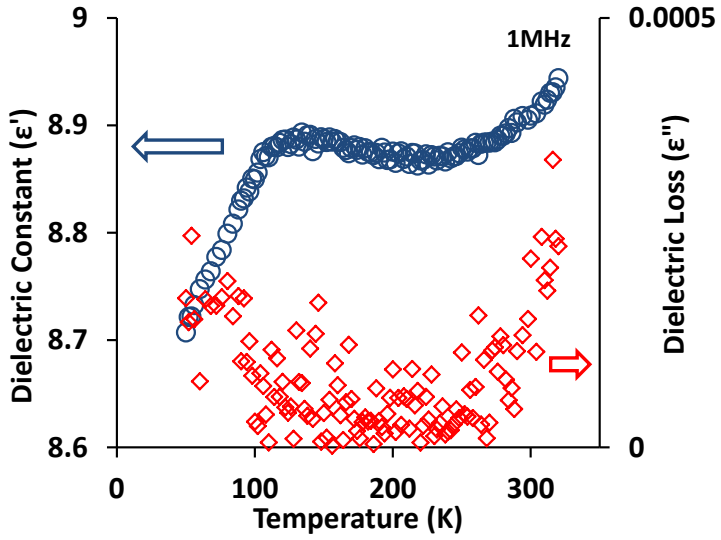


(b)

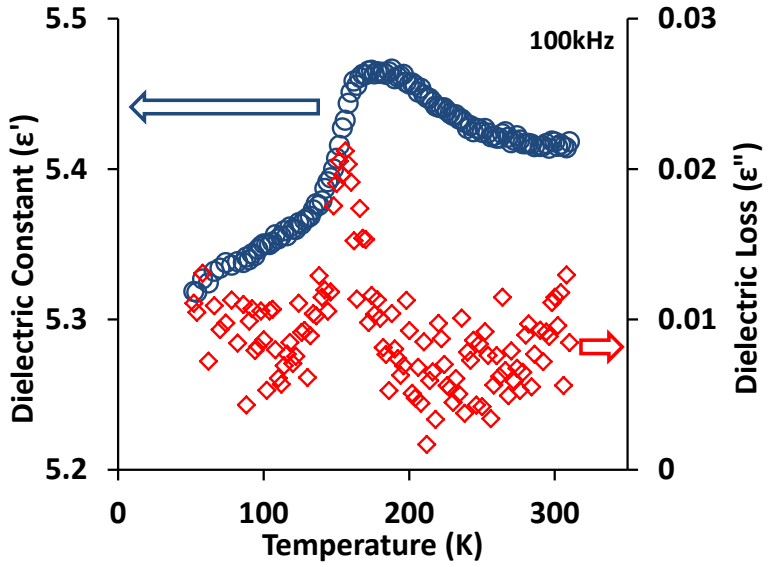


**Figure 7** Dielectric constant and loss for (a) $YFeO_3$ at 1MHz and (b) $YbFeO_3$ at 100kHz

(a)

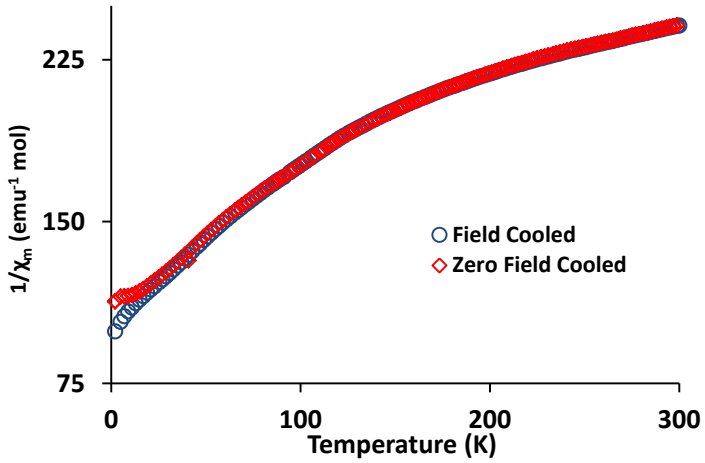


b)

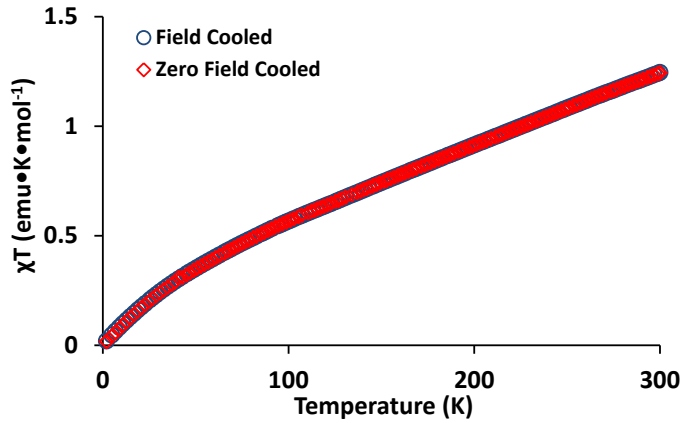


c)

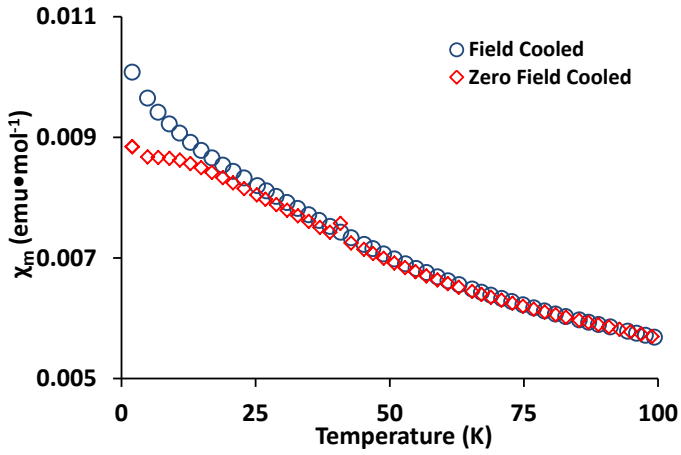


**Figure 8** (a) $1/\chi$ versus T (b) $\chi T$ versus T and (c) $\chi$ versus T for $YFeO_3$

a)

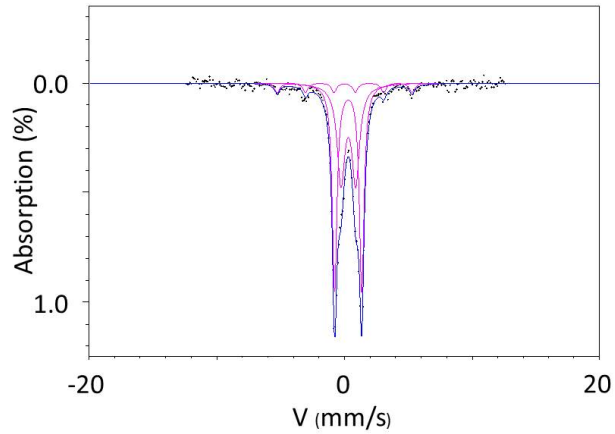


b)

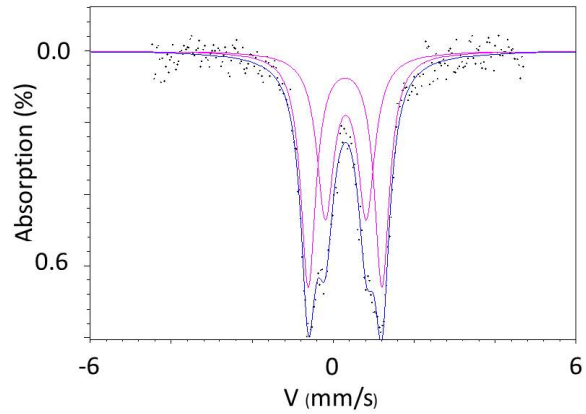


c)

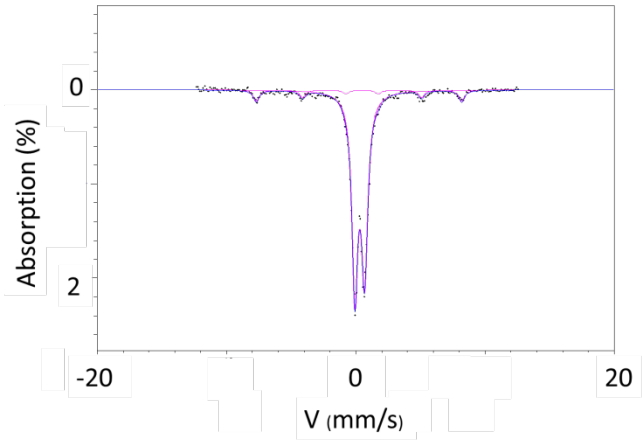


**Figure 9** Mössbauer spectra of (a) $YFeO_3$, (b) $YbFeO_3$ and (c) $InFeO_3$ at room temperature, showing fits as discussed in the text.

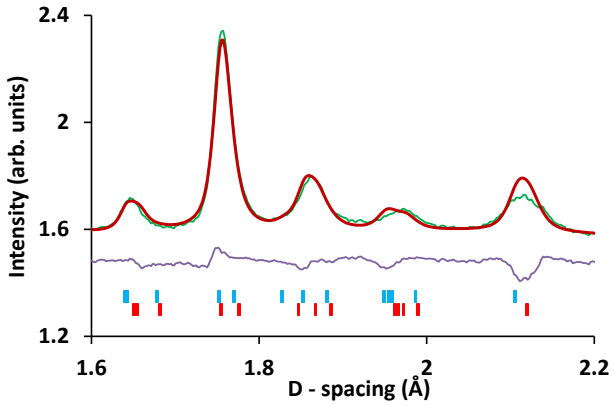


**Figure 10** Two–phase fit to the NPD data, using two 'identical' $P6_3cm$ models with different lattice parameters, for $YFeO_3$

(a)

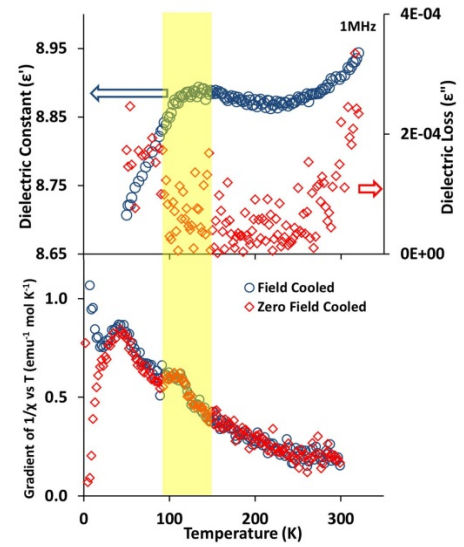


(b)

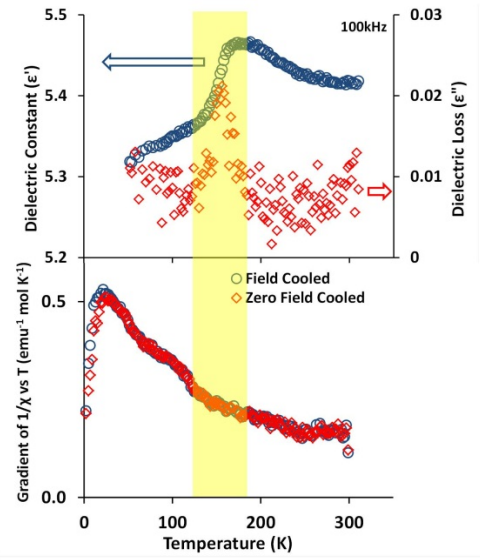


**Figure 11** (a) Dielectric data for $YFeO_3$ at 1 MHz showing low T anomaly centred at 150 K, and the corresponding anomaly in d(1/χ)/dT (b) Analogous data for $YbFeO_3$ at 100 kHz, with no apparent direct correspondence. The shaded area is a guide-to-the-eye only.

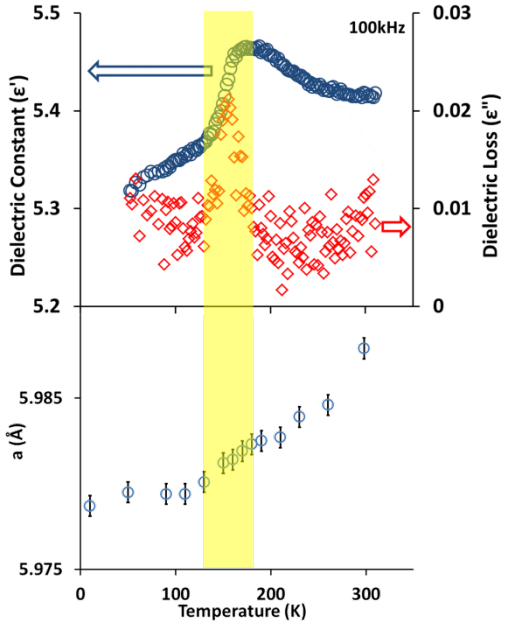


**Figure 12** Dielectric data and *a* lattice parameter for $YbFeO_3$

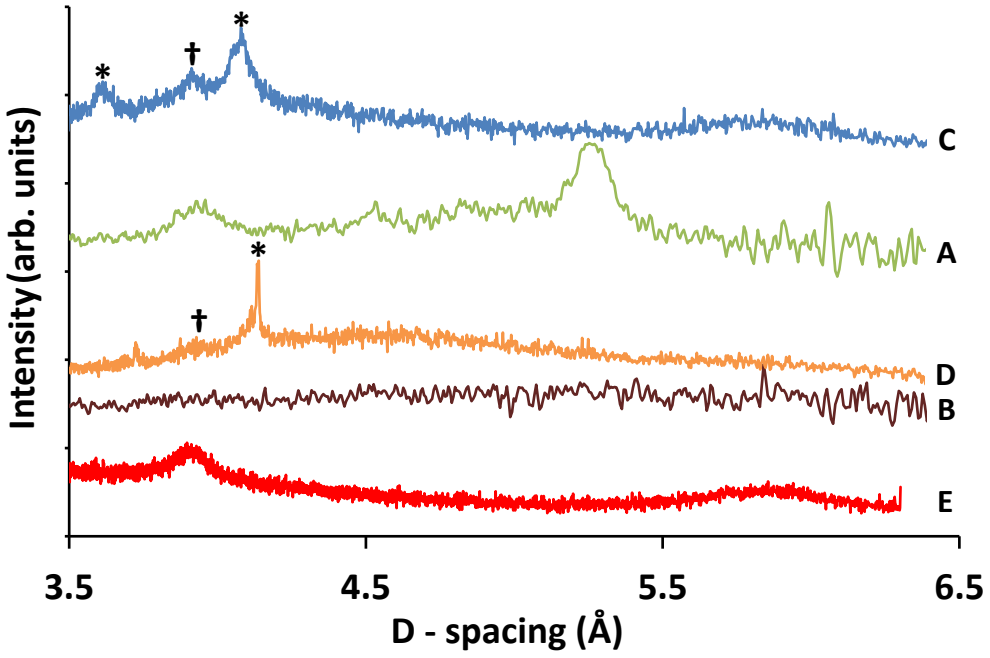


**Figure 13** Comparison plot of synchrotron X-ray powder patterns and neutron powder patterns for $YFeO_3$; A = NPD at 35 K, B = NPD at RT, C = PXRD at 30 K, D = PXRD at RT (cryostat set up), E = PXRD at RT (glass capillary set up) (Peaks marked * are due to sample environment and peaks marked † are allowed structural reflections).

(a)

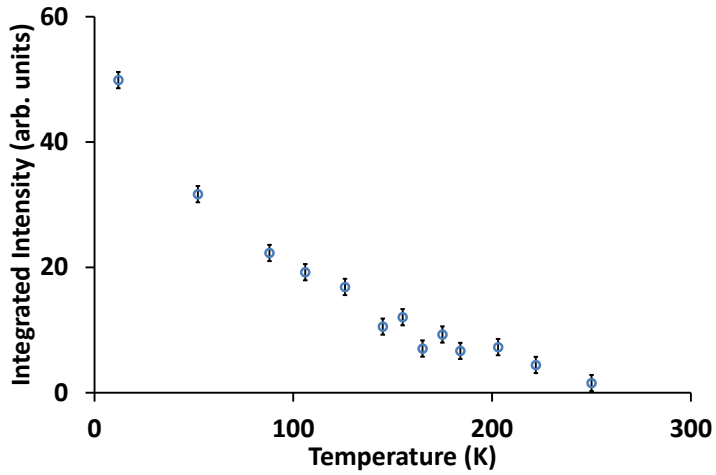


(b)

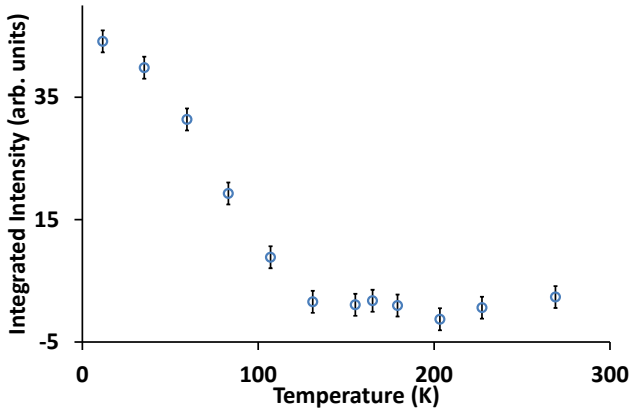


**Figure 14** Thermal evolution of the intensity of the (a) (100) magnetic peak for $YbFeO_3$, showing non-saturating behaviour $1/\chi_m$ and (b) thermal evolution of the intensity of the (100) magnetic peak for $YFeO_3$ showing saturating behaviour